Supplemental Material

Using Regionalized Air Quality Model Performance and Bayesian Maximum Entropy data fusion to map global surface ozone concentration

Jacob S. Becker[1], Marissa N. DeLang[1], Kai-Lan Chang[2,3], Marc L. Serre[1], Owen R. Cooper[2,3], Hantao Wang[1], Martin G. Schultz[4], Sabine Schröder[4], Xiao Lu[5], Lin Zhang[6], Makoto Deushi[7], Beatrice Josse[8], Christoph A. Keller[9,10], Jean-François Lamarque[11], Meiyun Lin[12,13], Junhua Liu[9,10], Virginie Marécal[8], Sarah A. Strode[9,10], Kengo Sudo[14,15], Simone Tilmes[11], Li Zhang[12,13,16], Michael Brauer[17,18], J. Jason West[*,1]

[1]Department of Environmental Sciences and Engineering, University of North Carolina at Chapel Hill, Chapel Hill, NC, USA

[2]Cooperative Institute for Research in Environmental Sciences, University of Colorado, Boulder, CO, USA

[3]NOAA Chemical Sciences Laboratory, Boulder, CO, USA

[4]Jülich Supercomputing Centre (JSC), Forschungszentrum Jülich, Jülich, Germany

[5]School of Atmospheric Sciences, Sun Yat-Sen University, Zhuhai, Guangdong, China

[6]Laboratory for Climate and Ocean-Atmosphere Studies, Department of Atmospheric and Oceanic Sciences, School of Physics, Peking University, Beijing, China

[7]Meteorological Research Institute (MRI), Tsukuba, Japan

[8]Centre National de Recherches Météorologiques, Université de Toulouse, Météo-France, CNRS, Toulouse, France

[9]NASA Goddard Space Flight Center, Greenbelt, MD, USA

[10]Universities Space Research Association, Columbia, MD, USA

[11]National Center for Atmospheric Research, Boulder, CO, USA

[12]NOAA Geophysical Fluid Dynamics Laboratory, Princeton, NJ, USA

[13]Program in Atmospheric and Oceanic Sciences, Princeton University, Princeton, NJ, USA

[14]Graduate School of Environmental Studies, Nagoya University, Nagoya, Japan

[15]Japan Agency for Marine-Earth Science and Technology (JAMSTEC), Yokosuka, Japan

[16]Department of Meteorology and Atmospheric Science, Pennsylvania State University, University Park, PA. USA

[17]Institute for Health Metrics and Evaluation, University of Washington, Seattle, Washington, USA

[18]School of Population and Public Health, University of British Columbia, Vancouver, British Columbia, Canada

* Corresponding Author: jasonwest@unc.edu

September 25, 2023

List of Contents:

Table S1. Differences in ozone estimates caused by including RAMP. Differences between ozone estimates are shown in the final case where weighted RAMP is used before BME data fusion, minus results without using RAMP, in ppb (the results of DeLang et al., 2021). Results are shown for 2000 and 2017, for average difference and the absolute value of differences, for area-weighted and population-weighted results, and for the mean, median, and 5^{th} / 95^{th} percentiles. A positive value indicates that results using weighted RAMP are higher. (page 28)

Table S2. Leave one out cross validation results. Results show that using RAMP decreases the mean square error (MSE) and increases R^2 over the M^3Fusion multi-model composite. When BME is used, the MSE and R^2 do not differ when using M^3Fusion as the global offset, or M^3Fusion bias-corrected using CAMP and weighted RAMP (wRAMP), which is expected because BME matches observations exactly at measurement stations, and many stations are clustered near one another. (page 30)

Text S1. Covariance description in Bayesian Maximum Entropy

The general knowledge $Y(\boldsymbol{p})$ includes the mean function $m_x(\boldsymbol{p}) = E[X]$, which is assumed to be zero due to the removal of the offset, and the covariance function $c_x(\boldsymbol{p},\boldsymbol{p}') = E[X(\boldsymbol{p})-m(\boldsymbol{p}))(X(\boldsymbol{p}')-m(\boldsymbol{p}')]$,which uses experimentally determined covariance of $\boldsymbol{r}_h$.

$$\hat{c}_X(r,\tau) \approx \frac{1}{N(x,\tau)}\sum_{i=1}^{N(x,\tau)} r_{head,i}\, r_{tail,i} - m_X^2$$

$N(x,\tau)$ is the number of pairs of points with values (r_{head}, r_{tail}) separated by spatial distance x and temporal distance τ, while m_x is the mean of r_0. We use an exponential covariance model for S/TRF Y(p) to fit:

$$c_X(r,\tau) = C\left[\gamma \exp\frac{-3r}{a_{r1}}\exp\frac{-3\tau}{a_{t1}} + \lambda \exp\frac{-3r}{a_{r2}}\exp\frac{-3\tau}{a_{t2}} + (1-\gamma-\lambda)\exp\frac{-3r}{a_{r3}}\exp\frac{-3\tau}{a_{t3}}\right]$$

Areas with a weight $w(\boldsymbol{p}) \geq 0.2$ used the RAMP derived covariance model (Figure S3a), while areas with $w(\boldsymbol{p}) < 0.2$ used the M^{3}Fusion derived covariance model, to insure a larger spatial range of influence for observations in areas without substantial RAMP correction (Figure S3b).

Figure S1. Complete annual results for each year from 1990 to 2017. Shown for each year are observations, estimates from the M^{3}Fusion composite, CAMP, RAMP, and wRAMP, and BME estimates with the M^{3}Fusion composite, CAMP, and wRAMP (our final estimates) as the global offset.

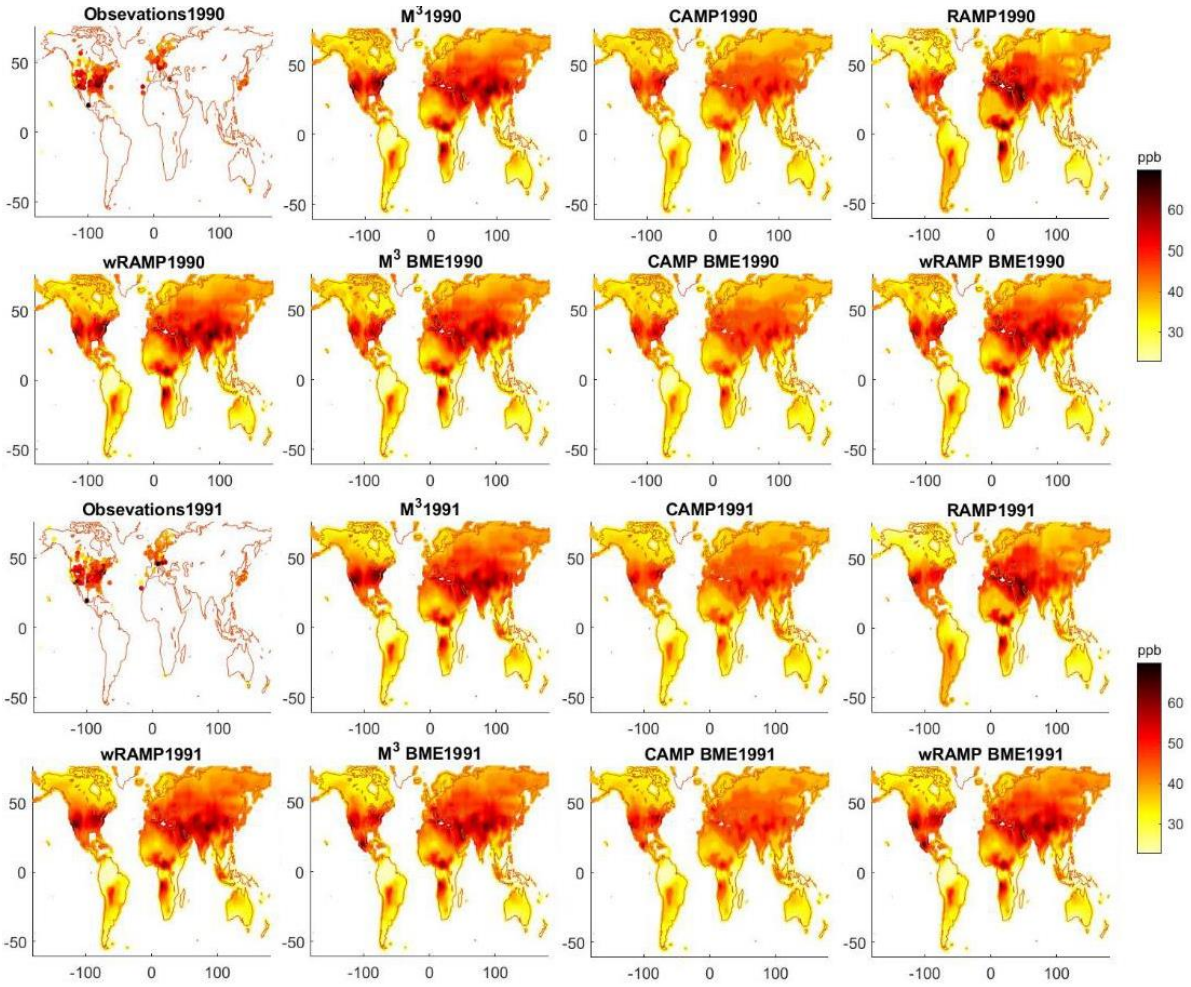

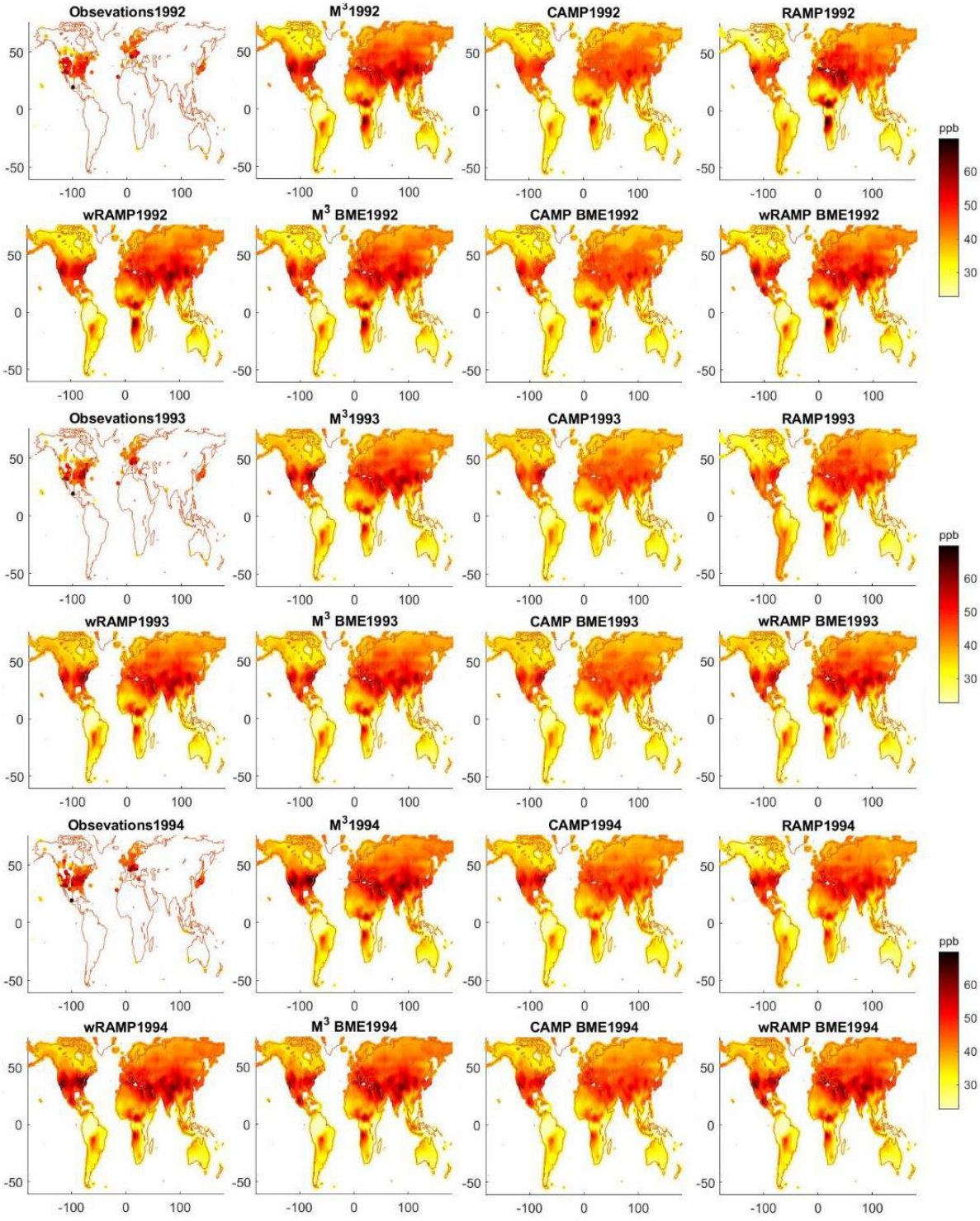
Obsevations1992
M3 1992
CAMP1992
RAMP1992
wRAMP1992
M3 BME1992
CAMP BME1992
wRAMP BME1992
Obsevations1993
M3 1993
CAMP1993
RAMP1993
wRAMP1993
M3 BME1993
CAMP BME1993
wRAMP BME1993
Obsevations1994
M3 1994
CAMP1994
RAMP1994
wRAMP1994
M3 BME1994
CAMP BME1994
wRAMP BME1994
ppb
60
50
40
30
50
0
-50
-100
0
100

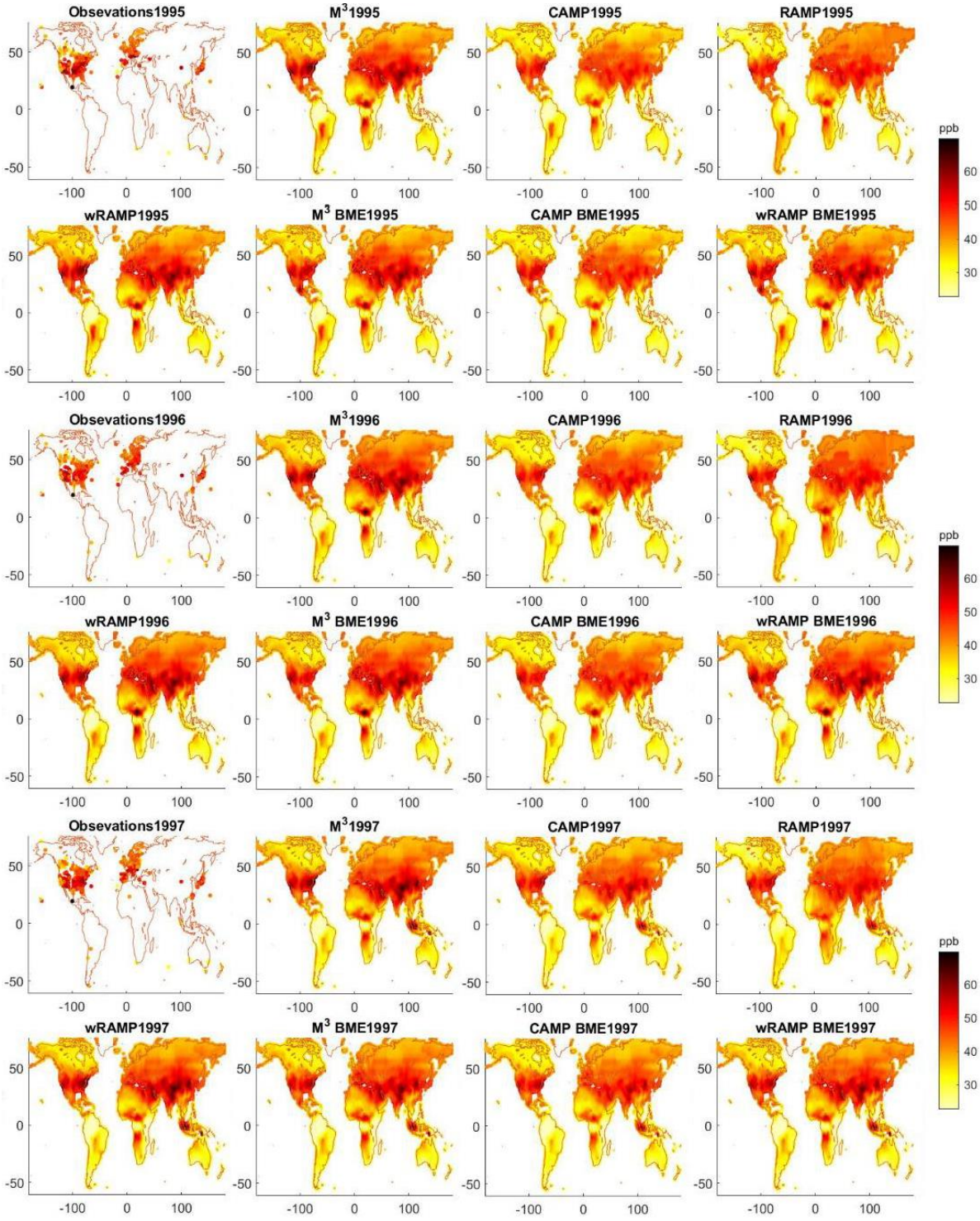
Obsevations1995
M31995
CAMP1995
RAMP1995
wRAMP1995
M3 BME1995
CAMP BME1995
wRAMP BME1995
Obsevations1996
M31996
CAMP1996
RAMP1996
wRAMP1996
M3 BME1996
CAMP BME1996
wRAMP BME1996
Obsevations1997
M31997
CAMP1997
RAMP1997
wRAMP1997
M3 BME1997
CAMP BME1997
wRAMP BME1997
ppb
60
50
40
30
50
0
-50
-100
0
100

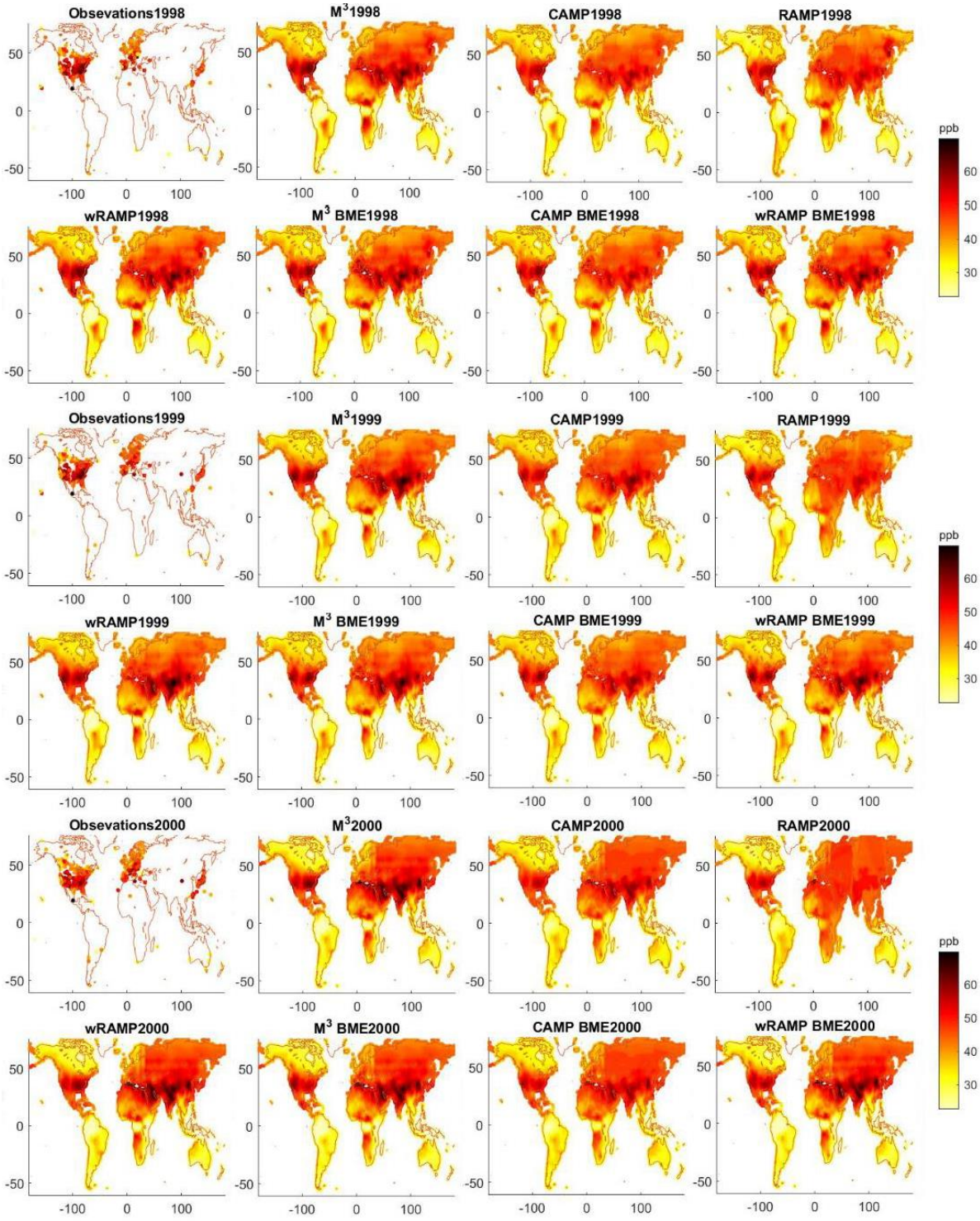
Obsevations1998
M31998
CAMP1998
RAMP1998
wRAMP1998
M3 BME1998
CAMP BME1998
wRAMP BME1998
Obsevations1999
M31999
CAMP1999
RAMP1999
wRAMP1999
M3 BME1999
CAMP BME1999
wRAMP BME1999
Obsevations2000
M32000
CAMP2000
RAMP2000
wRAMP2000
M3 BME2000
CAMP BME2000
wRAMP BME2000
ppb
60
50
40
30
50
0
-50
-100
0
100

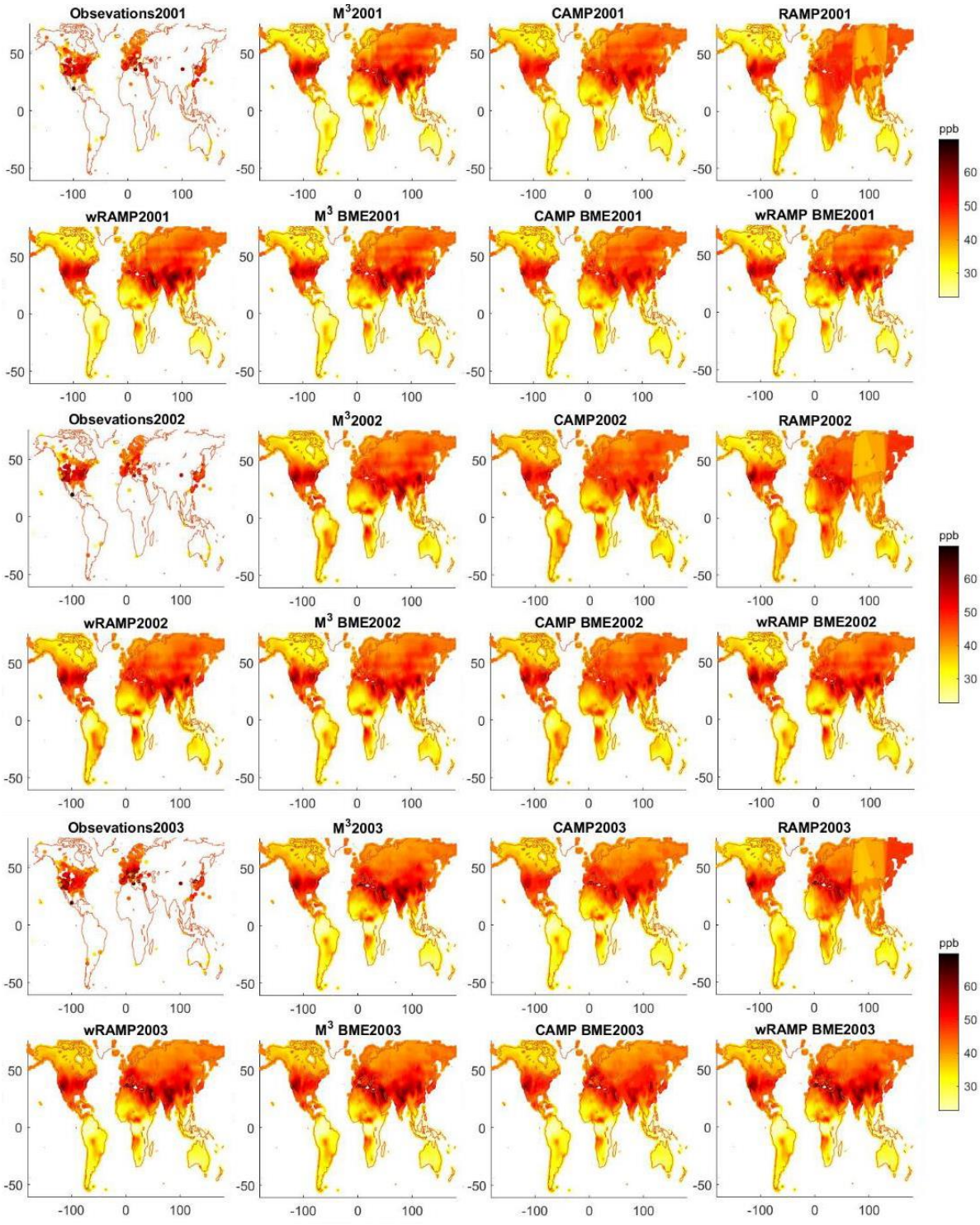
Obsevations2001
M32001
CAMP2001
RAMP2001
wRAMP2001
M3 BME2001
CAMP BME2001
wRAMP BME2001
Obsevations2002
M32002
CAMP2002
RAMP2002
wRAMP2002
M3 BME2002
CAMP BME2002
wRAMP BME2002
Obsevations2003
M32003
CAMP2003
RAMP2003
wRAMP2003
M3 BME2003
CAMP BME2003
wRAMP BME2003
ppb
60
50
40
30
50
0
-50
-100
0
100

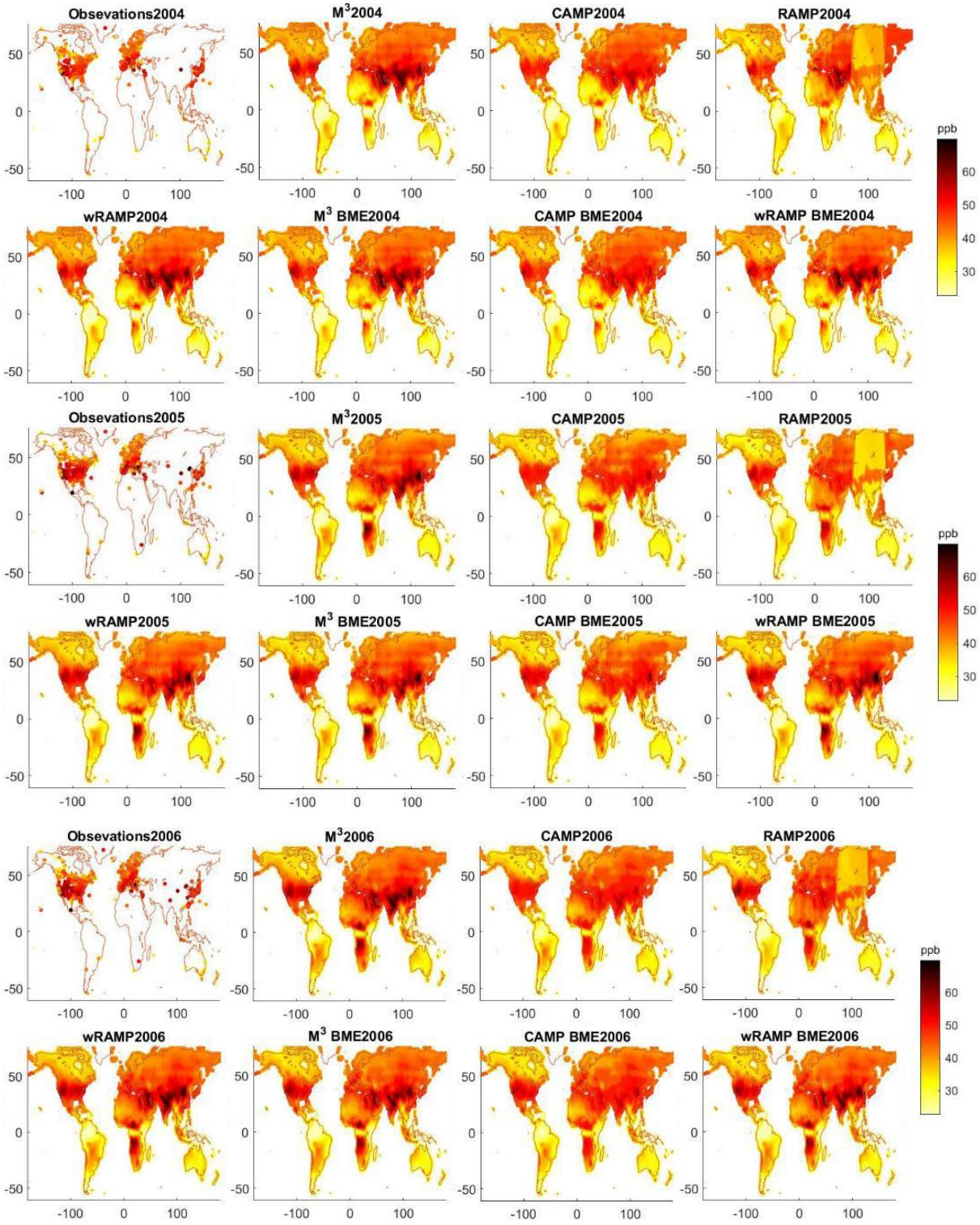
Obsevations2004
M32004
CAMP2004
RAMP2004
wRAMP2004
M3 BME2004
CAMP BME2004
wRAMP BME2004
Obsevations2005
M32005
CAMP2005
RAMP2005
wRAMP2005
M3 BME2005
CAMP BME2005
wRAMP BME2005
Obsevations2006
M32006
CAMP2006
RAMP2006
wRAMP2006
M3 BME2006
CAMP BME2006
wRAMP BME2006
ppb
60
50
40
30
50
0
-50
-100
0
100

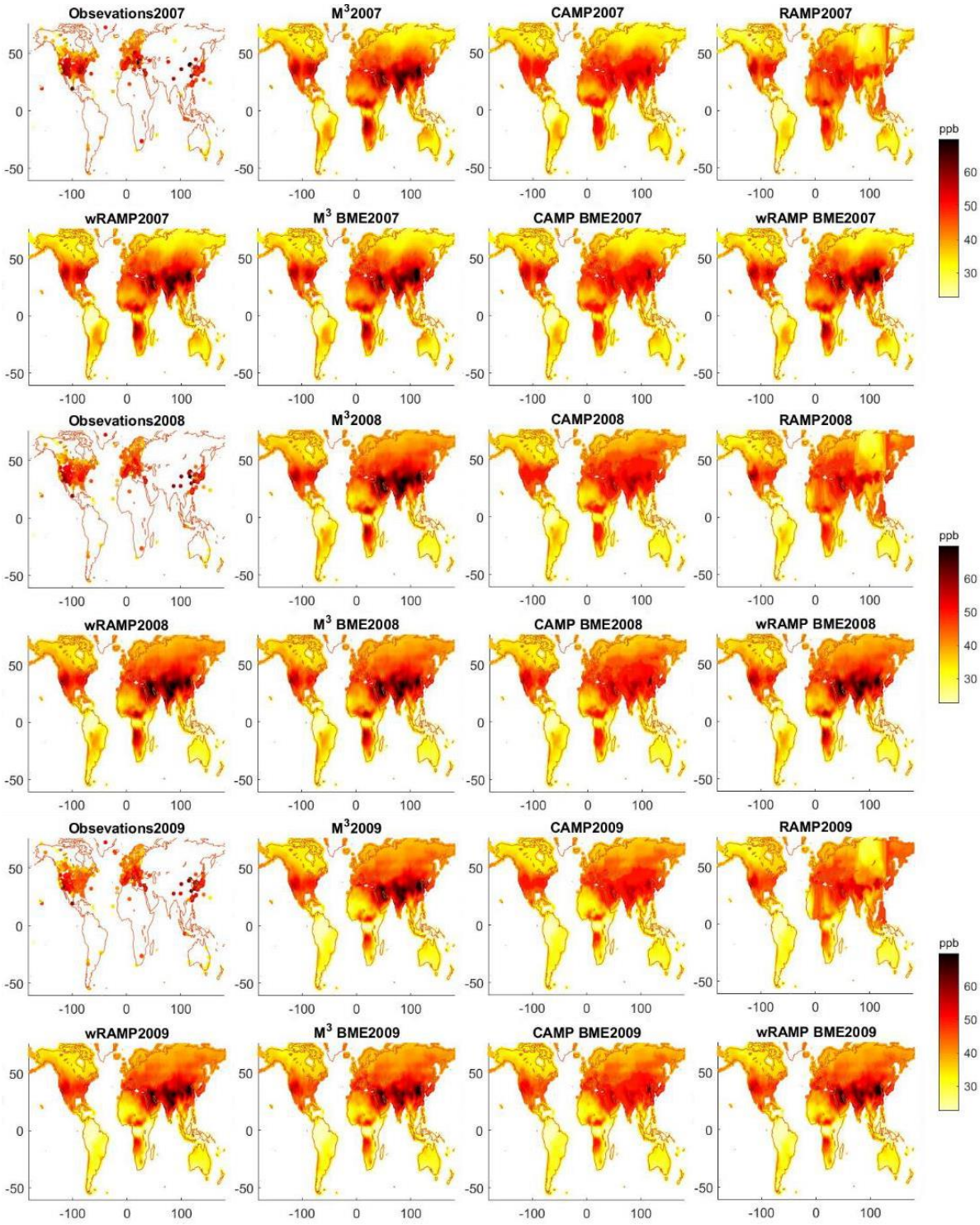
Obsevations2007
M32007
CAMP2007
RAMP2007
wRAMP2007
M3 BME2007
CAMP BME2007
wRAMP BME2007
Obsevations2008
M32008
CAMP2008
RAMP2008
wRAMP2008
M3 BME2008
CAMP BME2008
wRAMP BME2008
Obsevations2009
M32009
CAMP2009
RAMP2009
wRAMP2009
M3 BME2009
CAMP BME2009
wRAMP BME2009
ppb
60
50
40
30
50
0
-50
-100
0
100

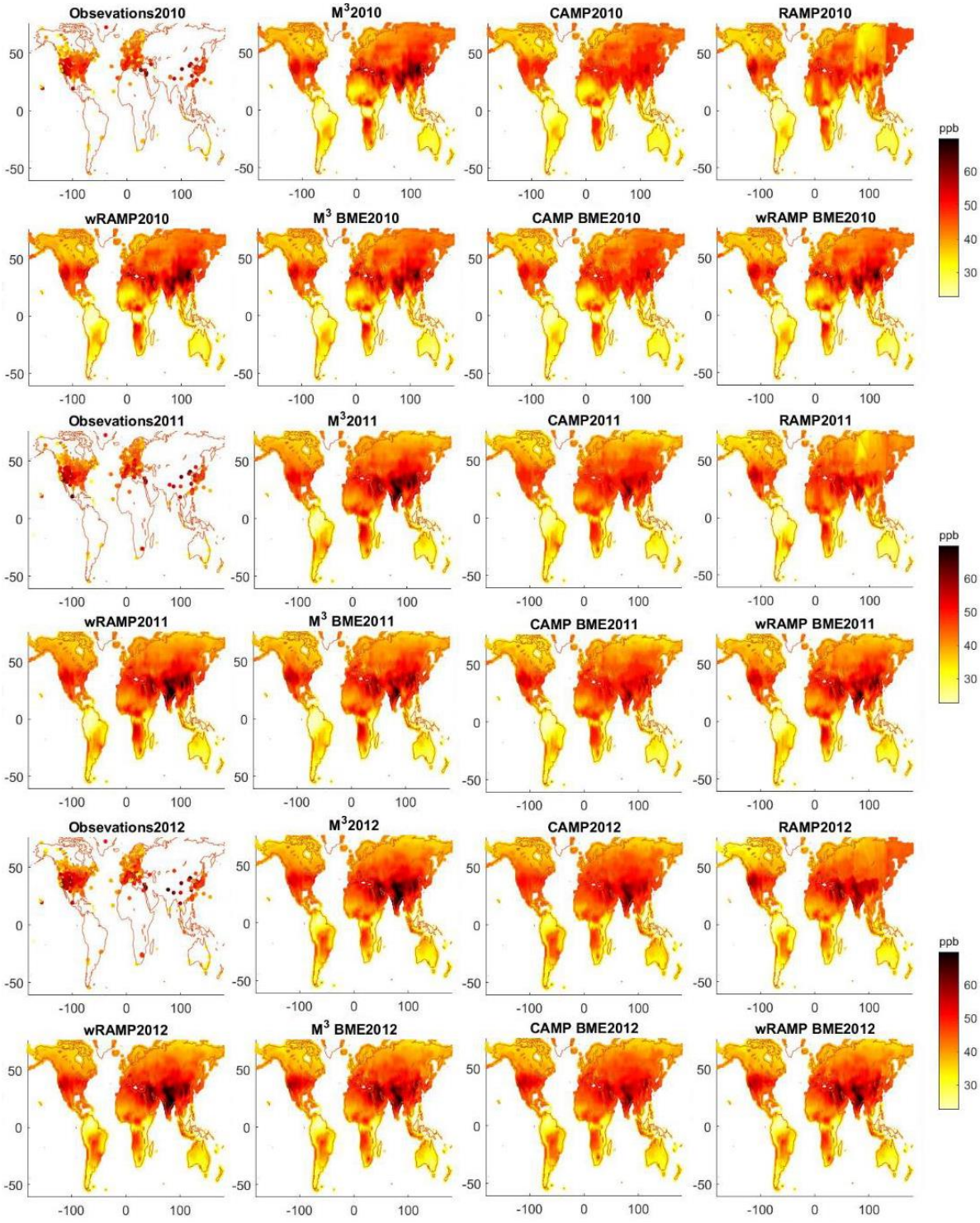
Obsevations2010
M32010
CAMP2010
RAMP2010
wRAMP2010
M3 BME2010
CAMP BME2010
wRAMP BME2010
Obsevations2011
M32011
CAMP2011
RAMP2011
wRAMP2011
M3 BME2011
CAMP BME2011
wRAMP BME2011
Obsevations2012
M32012
CAMP2012
RAMP2012
wRAMP2012
M3 BME2012
CAMP BME2012
wRAMP BME2012
ppb
60
50
40
30
50
0
-50
-100
0
100

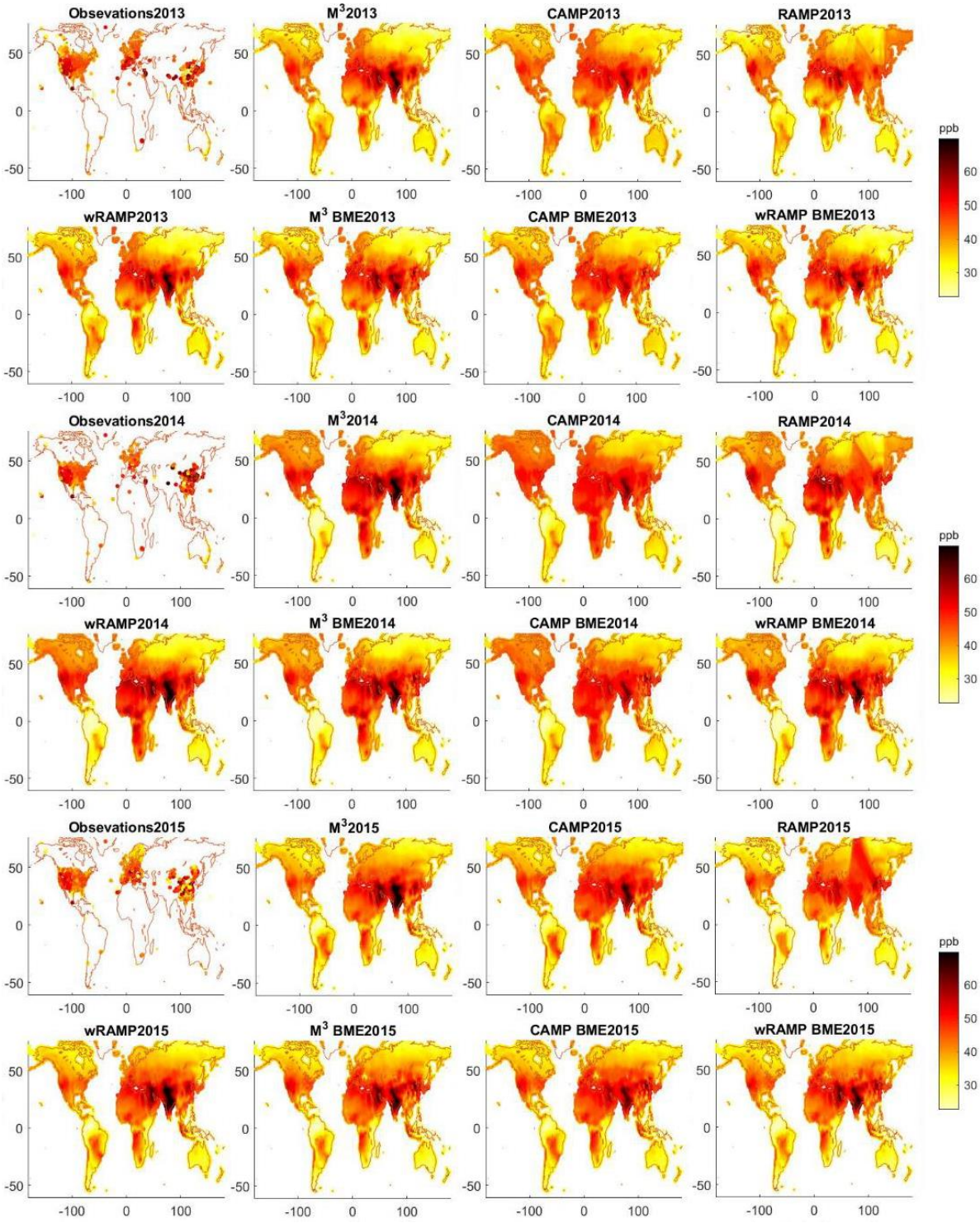
Obsevations2013
M32013
CAMP2013
RAMP2013
wRAMP2013
M3 BME2013
CAMP BME2013
wRAMP BME2013
Obsevations2014
M32014
CAMP2014
RAMP2014
wRAMP2014
M3 BME2014
CAMP BME2014
wRAMP BME2014
Obsevations2015
M32015
CAMP2015
RAMP2015
wRAMP2015
M3 BME2015
CAMP BME2015
wRAMP BME2015
ppb
60
50
40
30
50
0
-50
-100
0
100

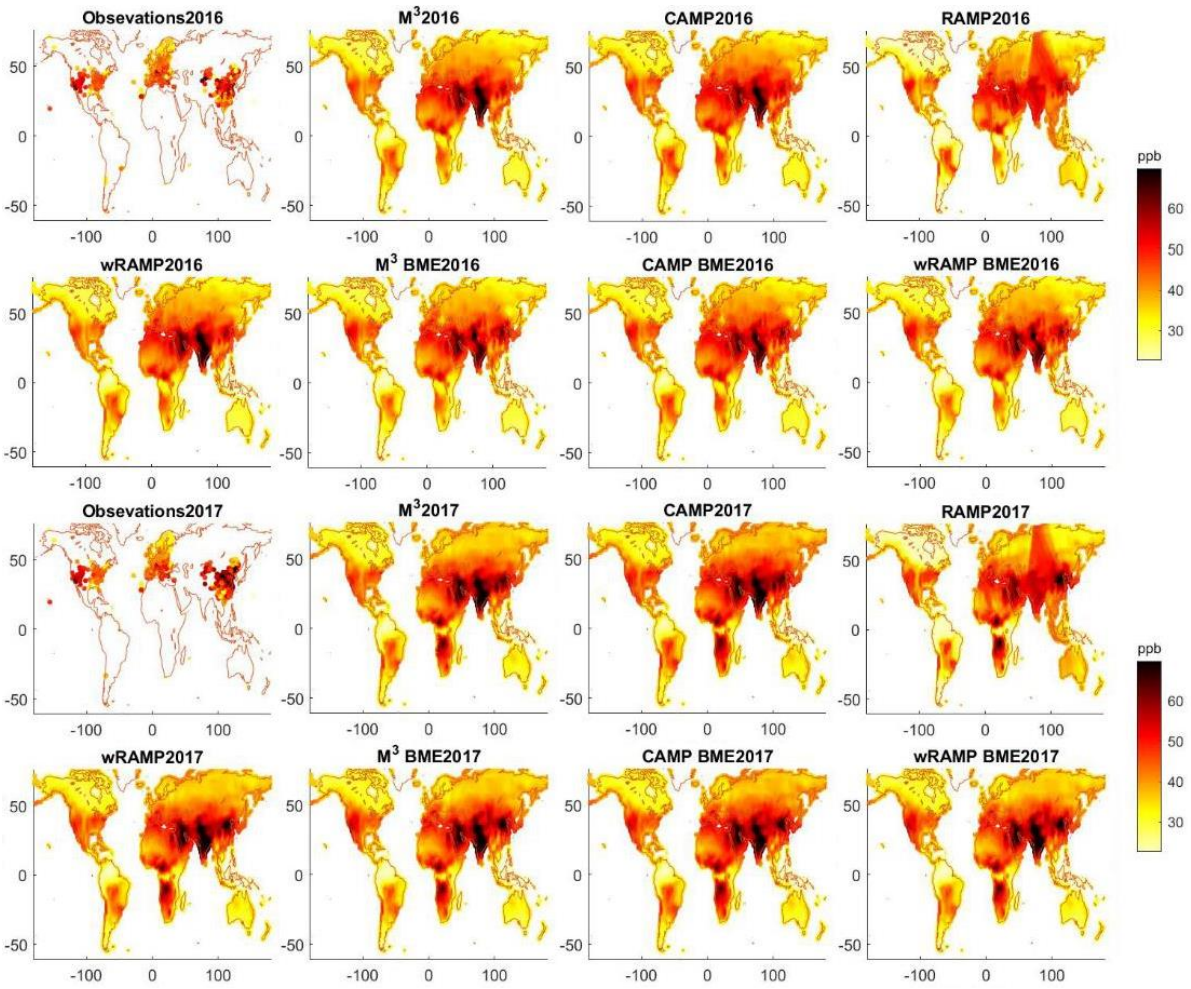
Obsevations2016
M32016
CAMP2016
RAMP2016
wRAMP2016
M3 BME2016
CAMP BME2016
wRAMP BME2016
Obsevations2017
M32017
CAMP2017
RAMP2017
wRAMP2017
M3 BME2017
CAMP BME2017
wRAMP BME2017
ppb
60
50
40
30
50
0
-50
-100
0
100

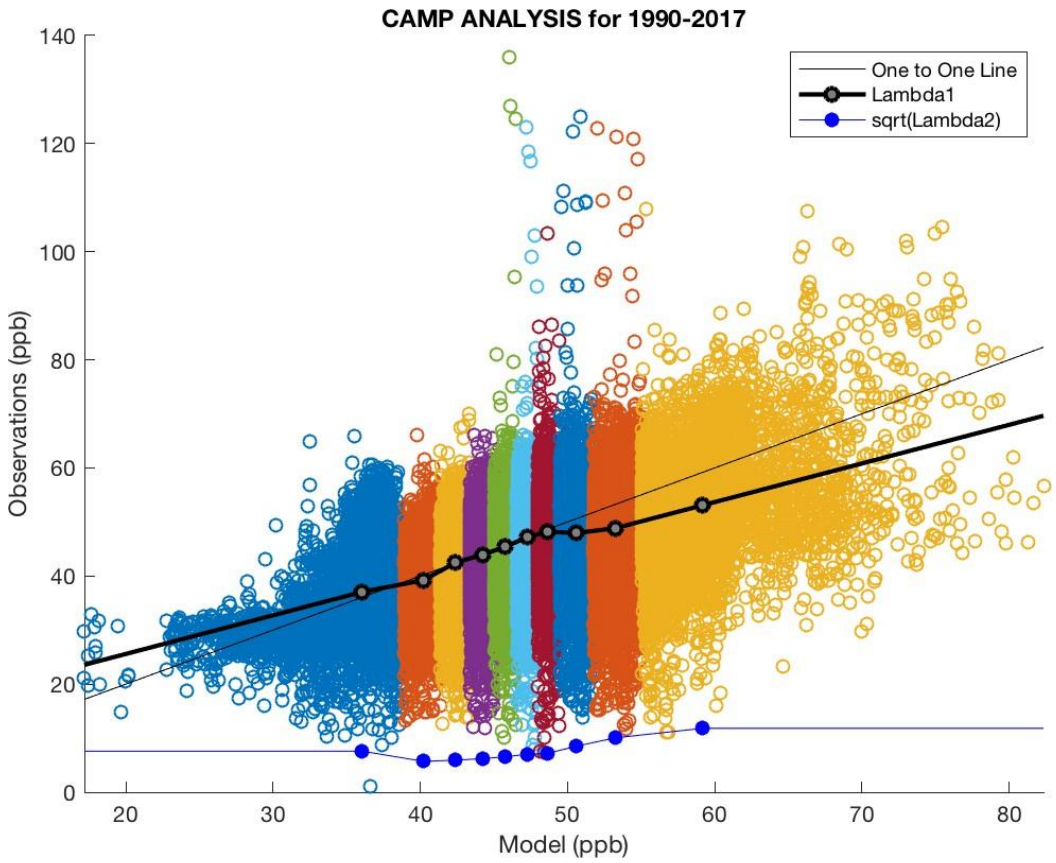

Figure S2. CAMP analysis for all years.

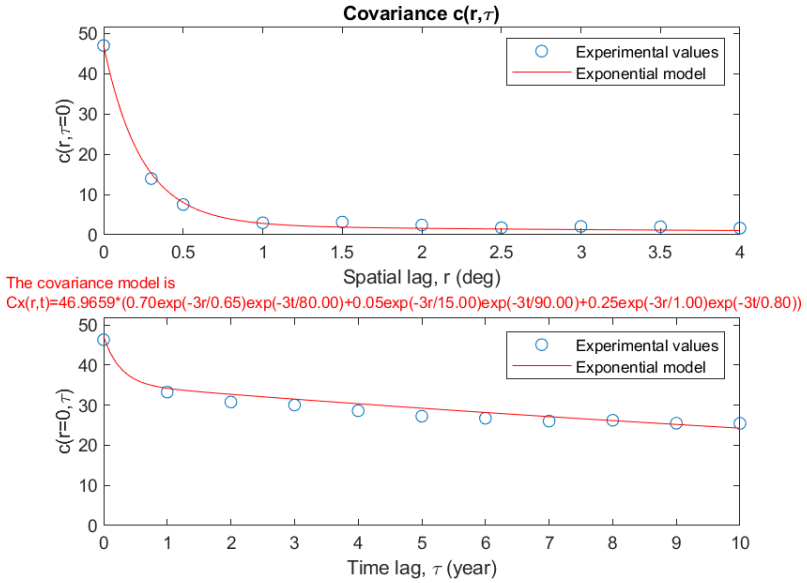

a)

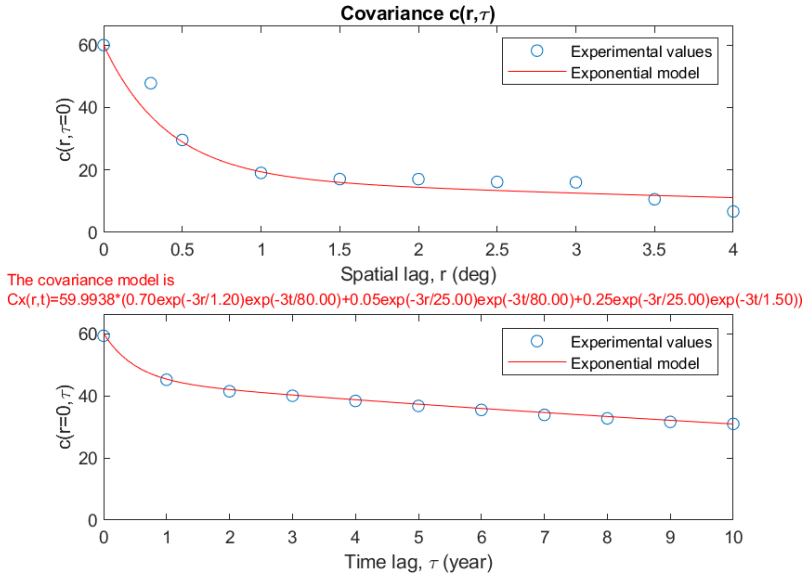

b)

Figure S3. Space/time covariance equations and graphs. a) is based on the RAMP corrected model, while b) is based solely on M^{3}Fusion. Both are used in BME estimation based on RAMP weight at a given location.

Figure S4. The BME variance each year under different configurations. Shown are the BME variance when the M^{3}Fusion composite, CAMP, and wRAMP are used as global offsets.

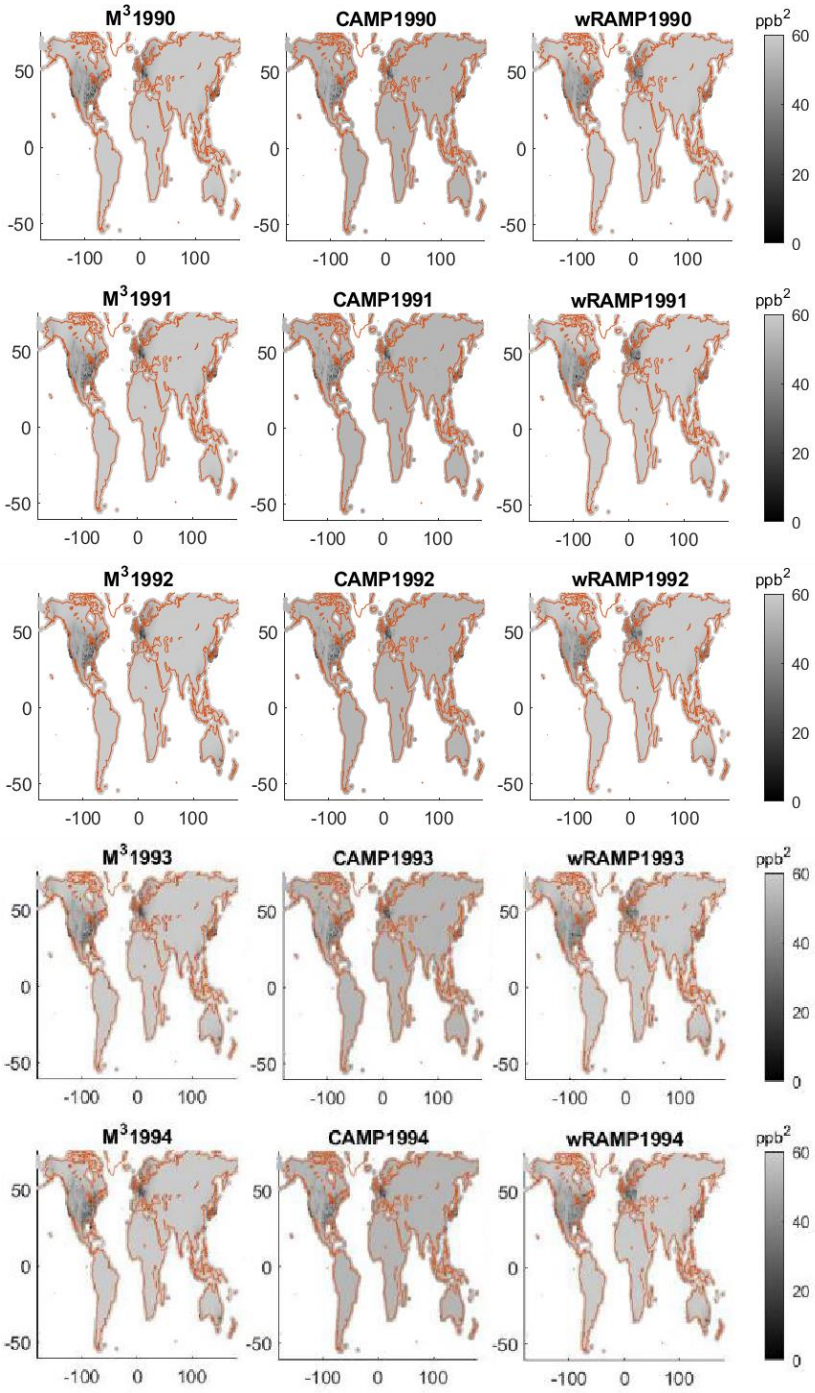

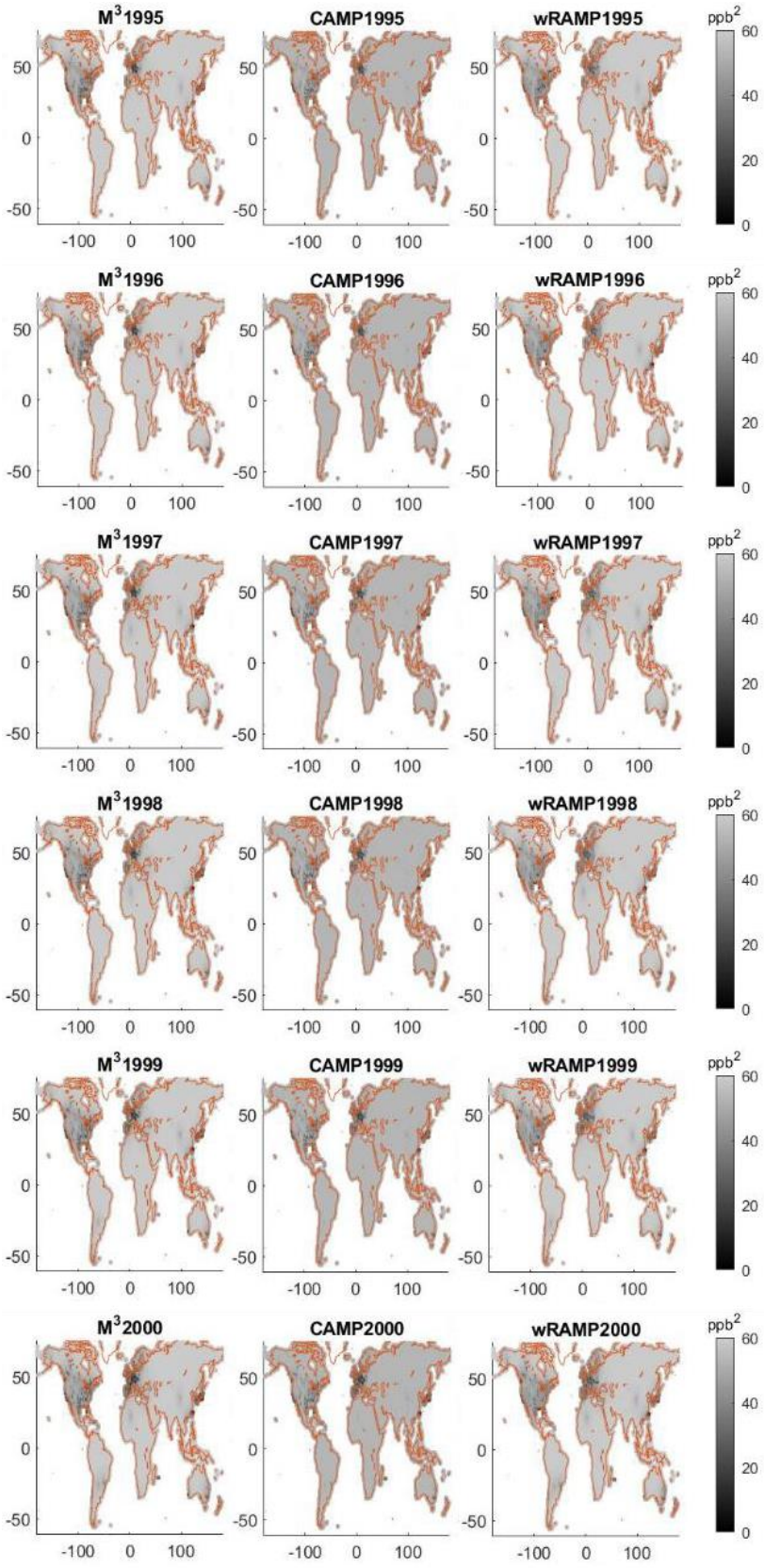
M³1995
CAMP1995
wRAMP1995
M³1996
CAMP1996
wRAMP1996
M³1997
CAMP1997
wRAMP1997
M³1998
CAMP1998
wRAMP1998
M³1999
CAMP1999
wRAMP1999
M³2000
CAMP2000
wRAMP2000
ppb²
60
40
20
0
50
0
-50
-100
0
100

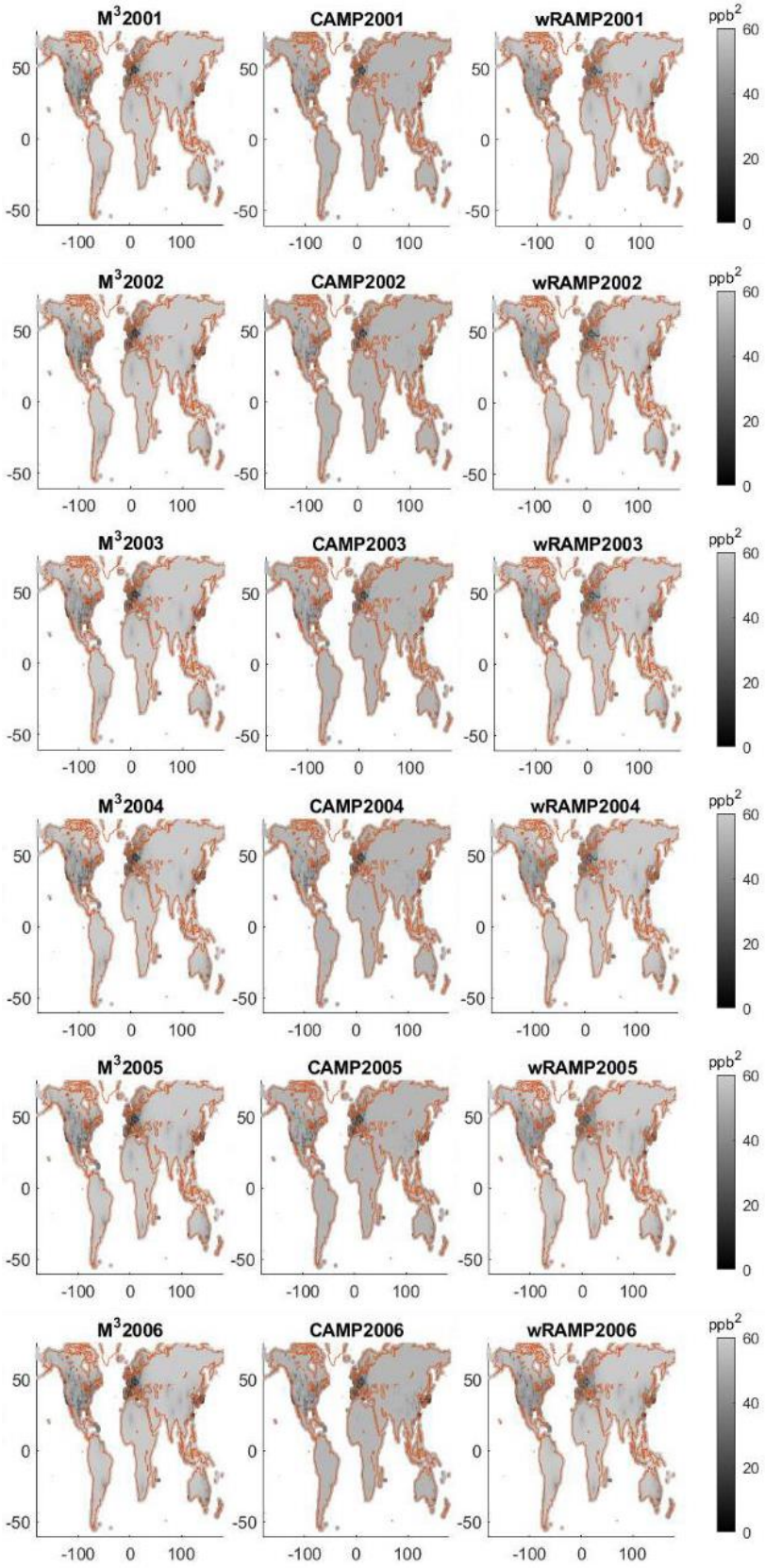
M32001
CAMP2001
wRAMP2001
M32002
CAMP2002
wRAMP2002
M32003
CAMP2003
wRAMP2003
M32004
CAMP2004
wRAMP2004
M32005
CAMP2005
wRAMP2005
M32006
CAMP2006
wRAMP2006
ppb2
60
40
20
0
50
0
-50
-100
0
100

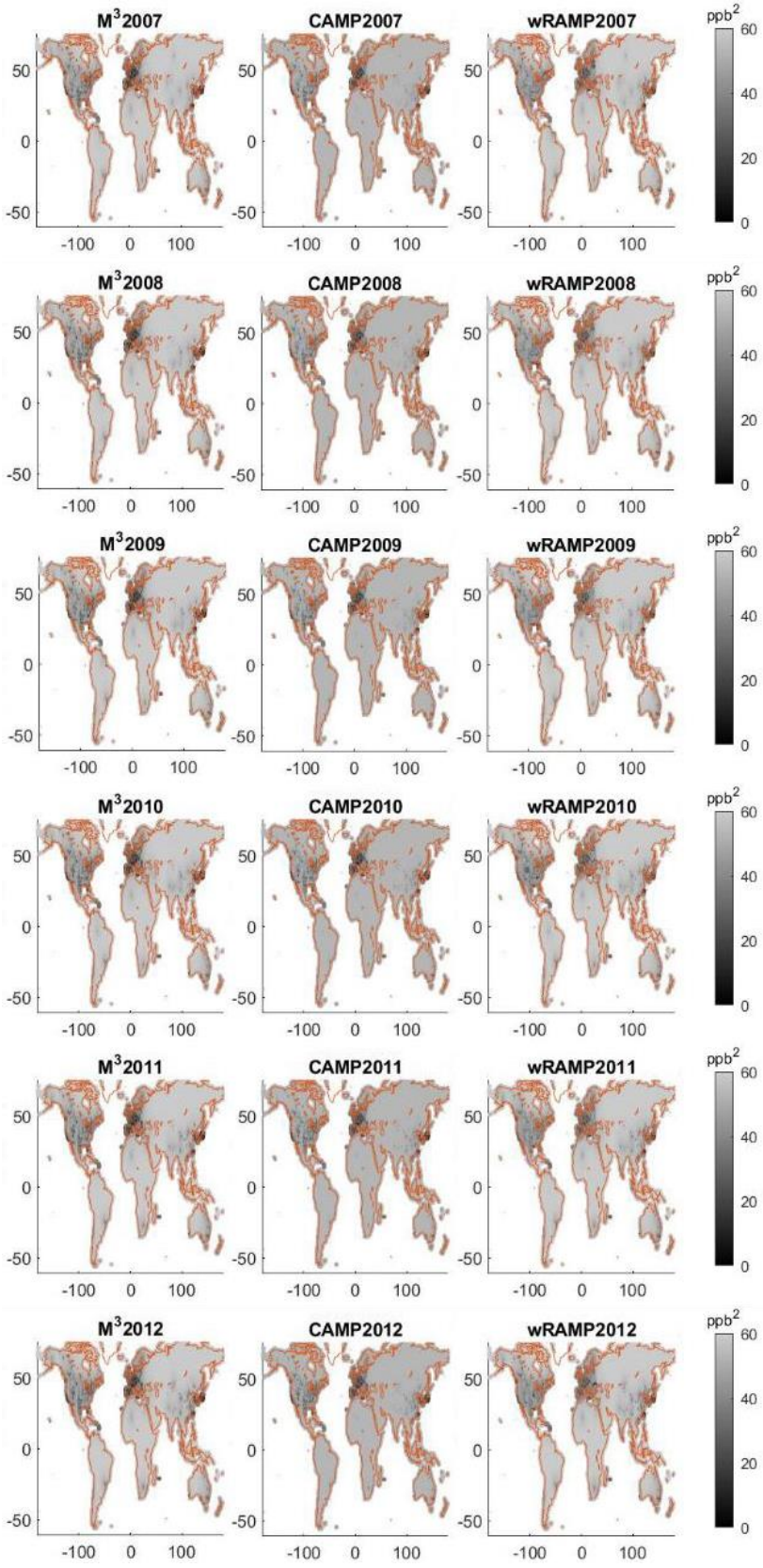
M32007
CAMP2007
wRAMP2007
M32008
CAMP2008
wRAMP2008
M32009
CAMP2009
wRAMP2009
M32010
CAMP2010
wRAMP2010
M32011
CAMP2011
wRAMP2011
M32012
CAMP2012
wRAMP2012
ppb2
60
40
20
0
50
0
-50
-100
0
100

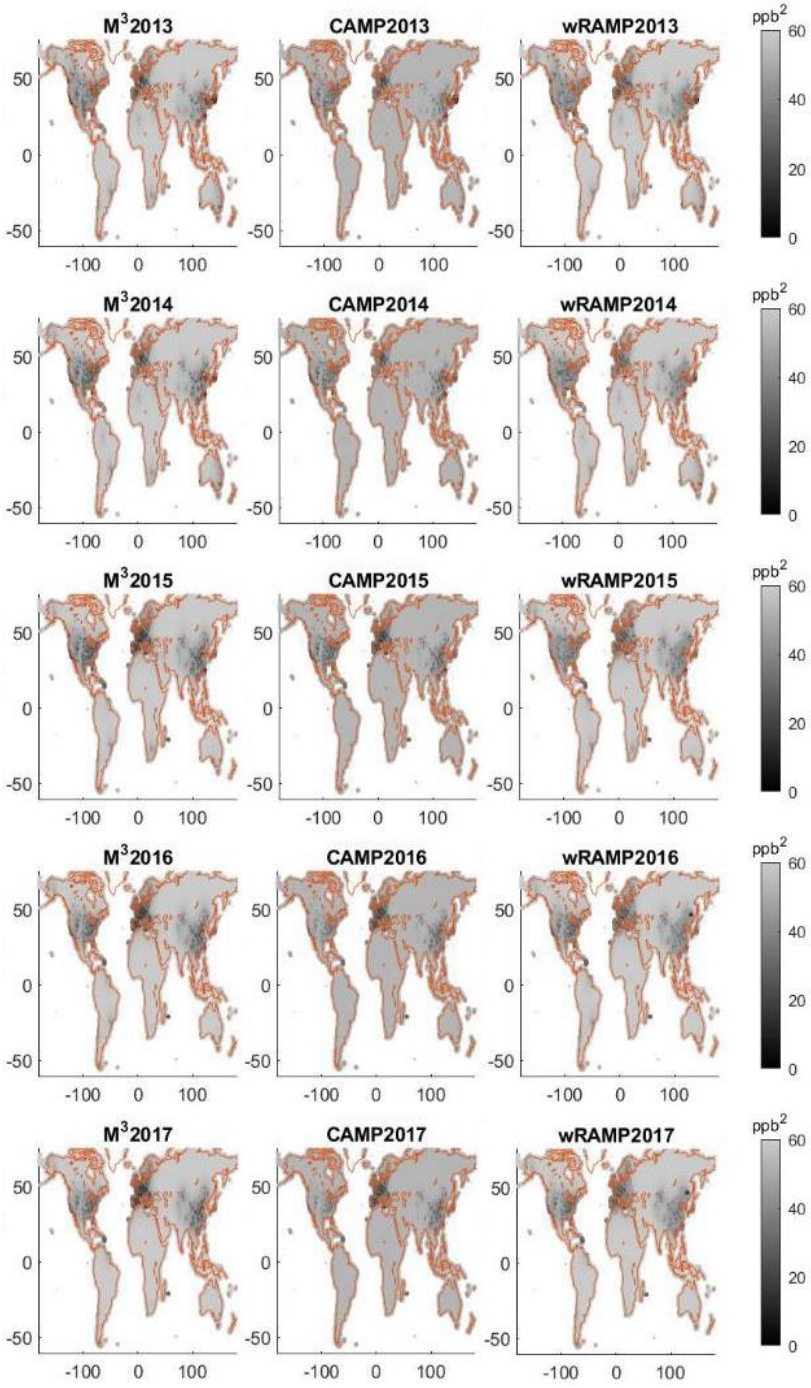
M32013
CAMP2013
wRAMP2013
M32014
CAMP2014
wRAMP2014
M32015
CAMP2015
wRAMP2015
M32016
CAMP2016
wRAMP2016
M32017
CAMP2017
wRAMP2017
ppb2
60
40
20
0
50
0
-50
-100
0
100

Figure S5. The likelilhood of exceedance of OSDMA8 at selected levels. Results are shown for each year 1990 to 2017, based on BME with wRAMP as the global offset.

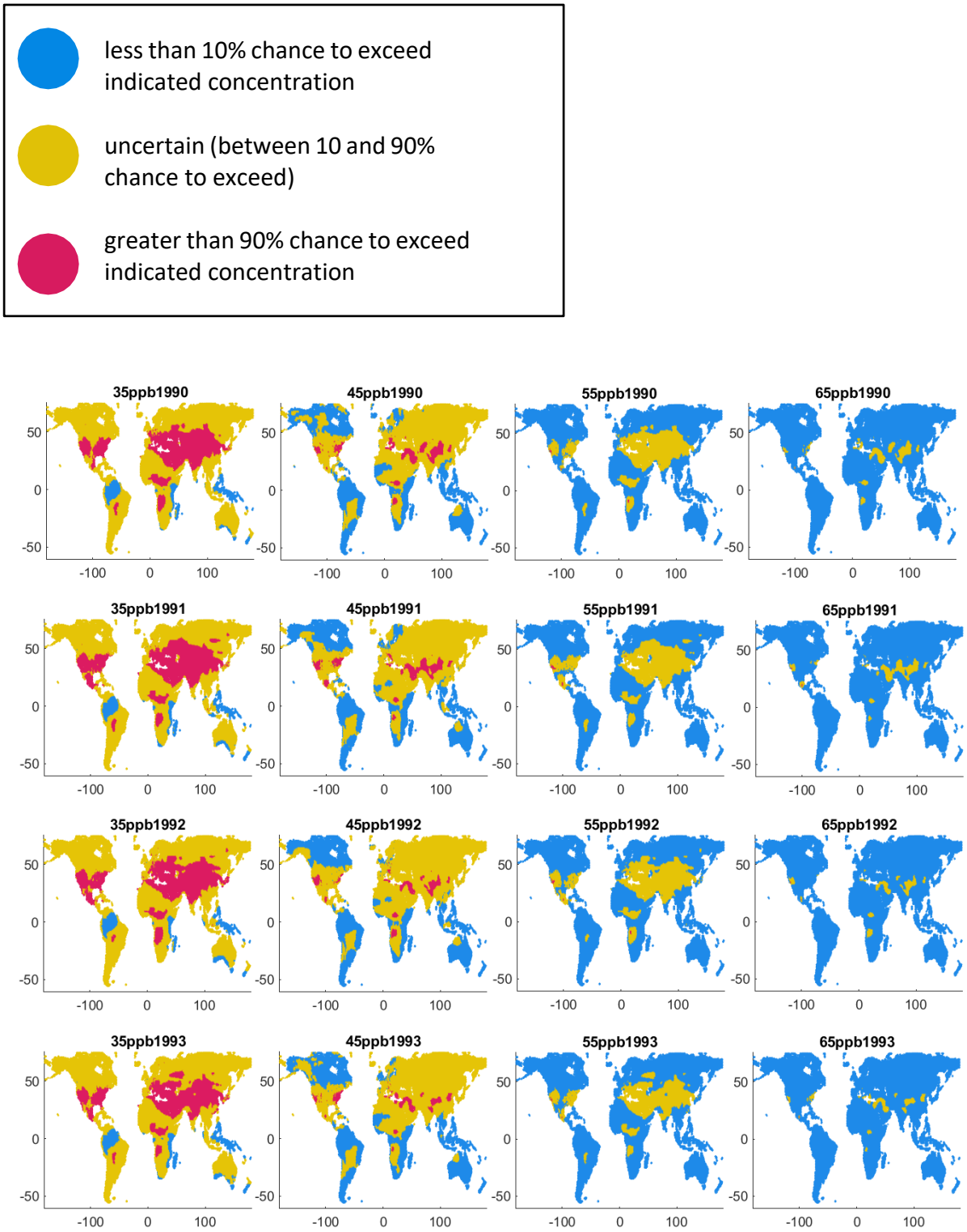

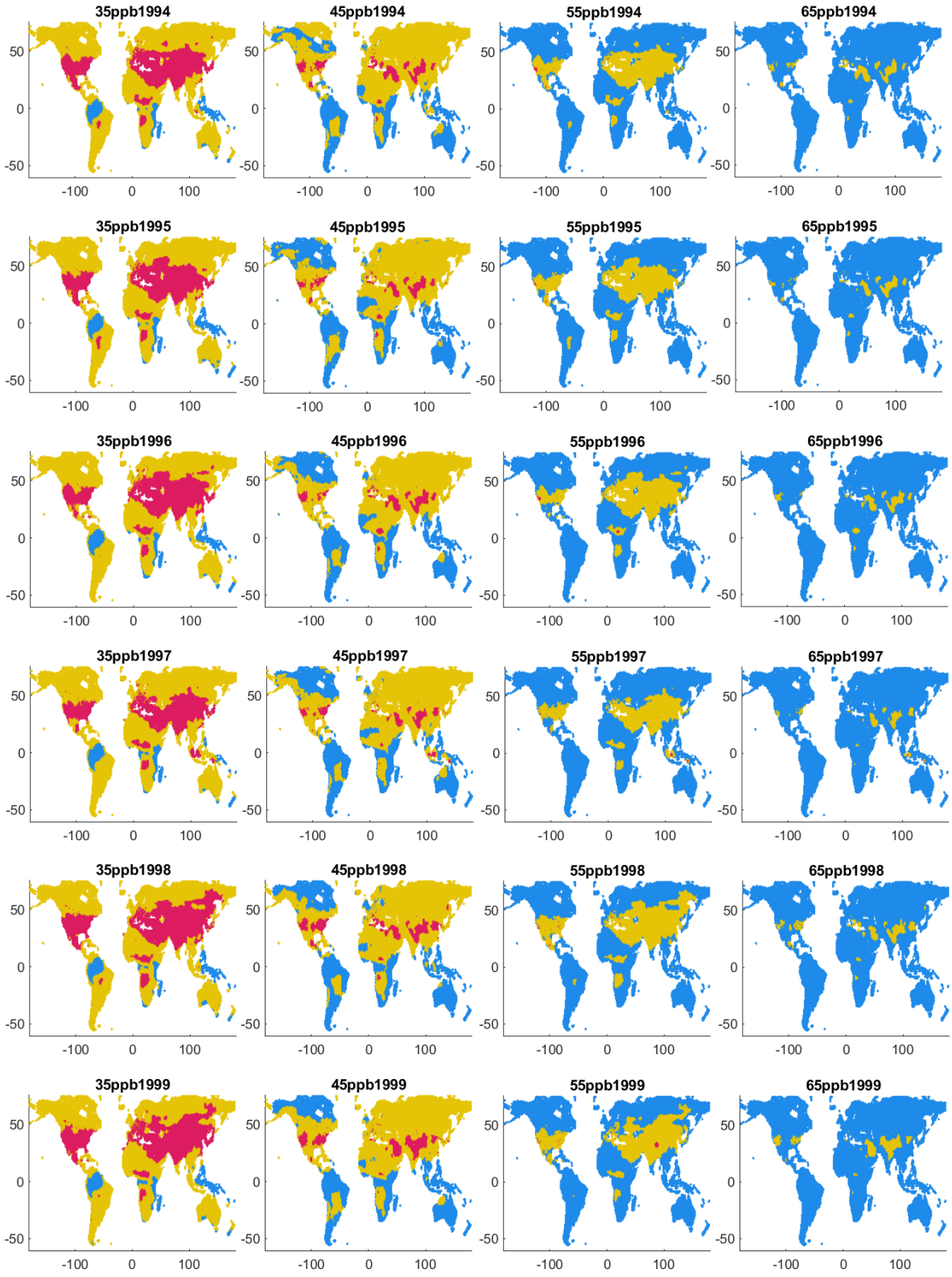
35ppb1994
45ppb1994
55ppb1994
65ppb1994
35ppb1995
45ppb1995
55ppb1995
65ppb1995
35ppb1996
45ppb1996
55ppb1996
65ppb1996
35ppb1997
45ppb1997
55ppb1997
65ppb1997
35ppb1998
45ppb1998
55ppb1998
65ppb1998
35ppb1999
45ppb1999
55ppb1999
65ppb1999
50
0
-50
-100
0
100

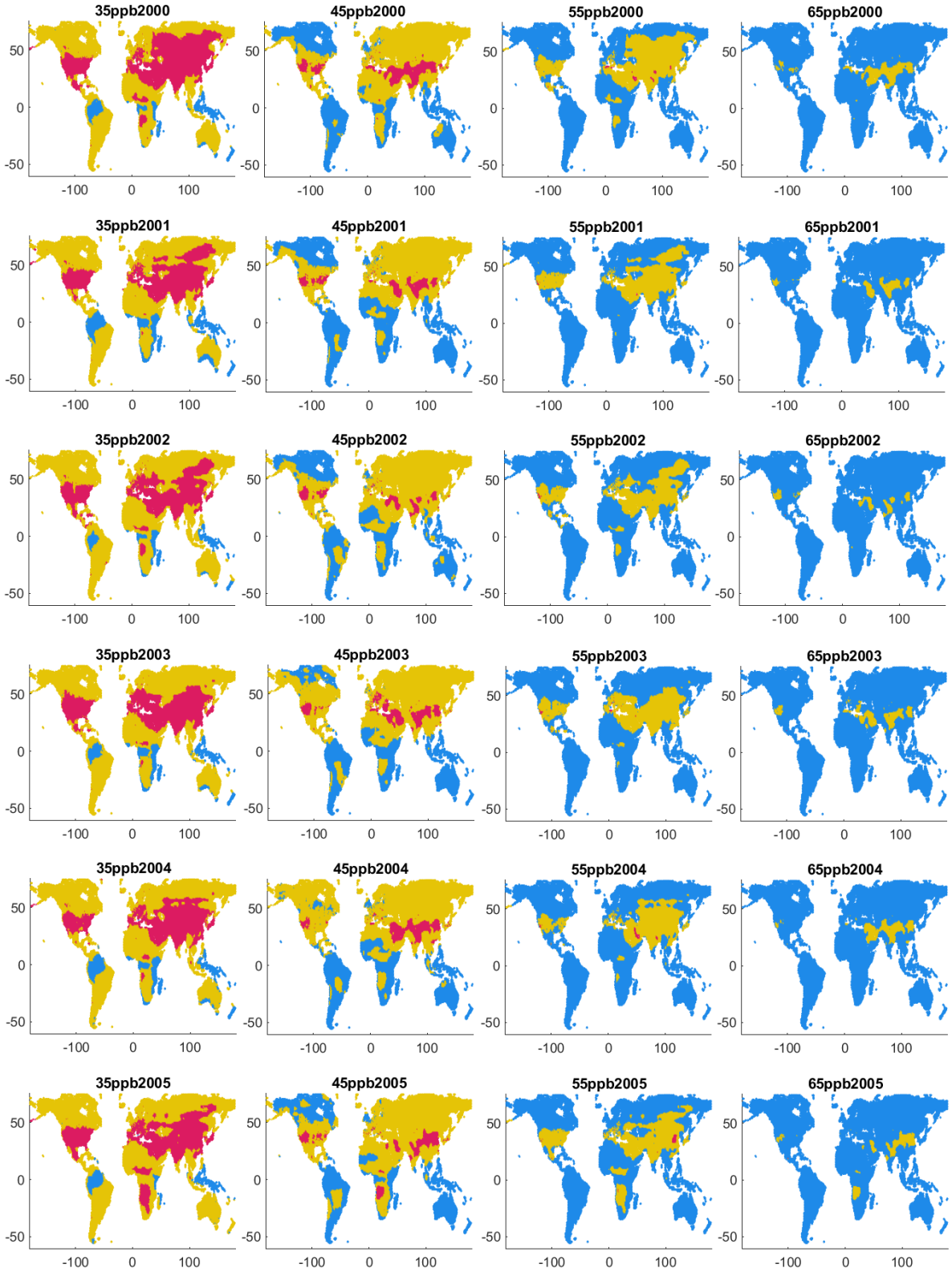
35ppb2000
45ppb2000
55ppb2000
65ppb2000
35ppb2001
45ppb2001
55ppb2001
65ppb2001
35ppb2002
45ppb2002
55ppb2002
65ppb2002
35ppb2003
45ppb2003
55ppb2003
65ppb2003
35ppb2004
45ppb2004
55ppb2004
65ppb2004
35ppb2005
45ppb2005
55ppb2005
65ppb2005
50
0
-50
-100
0
100

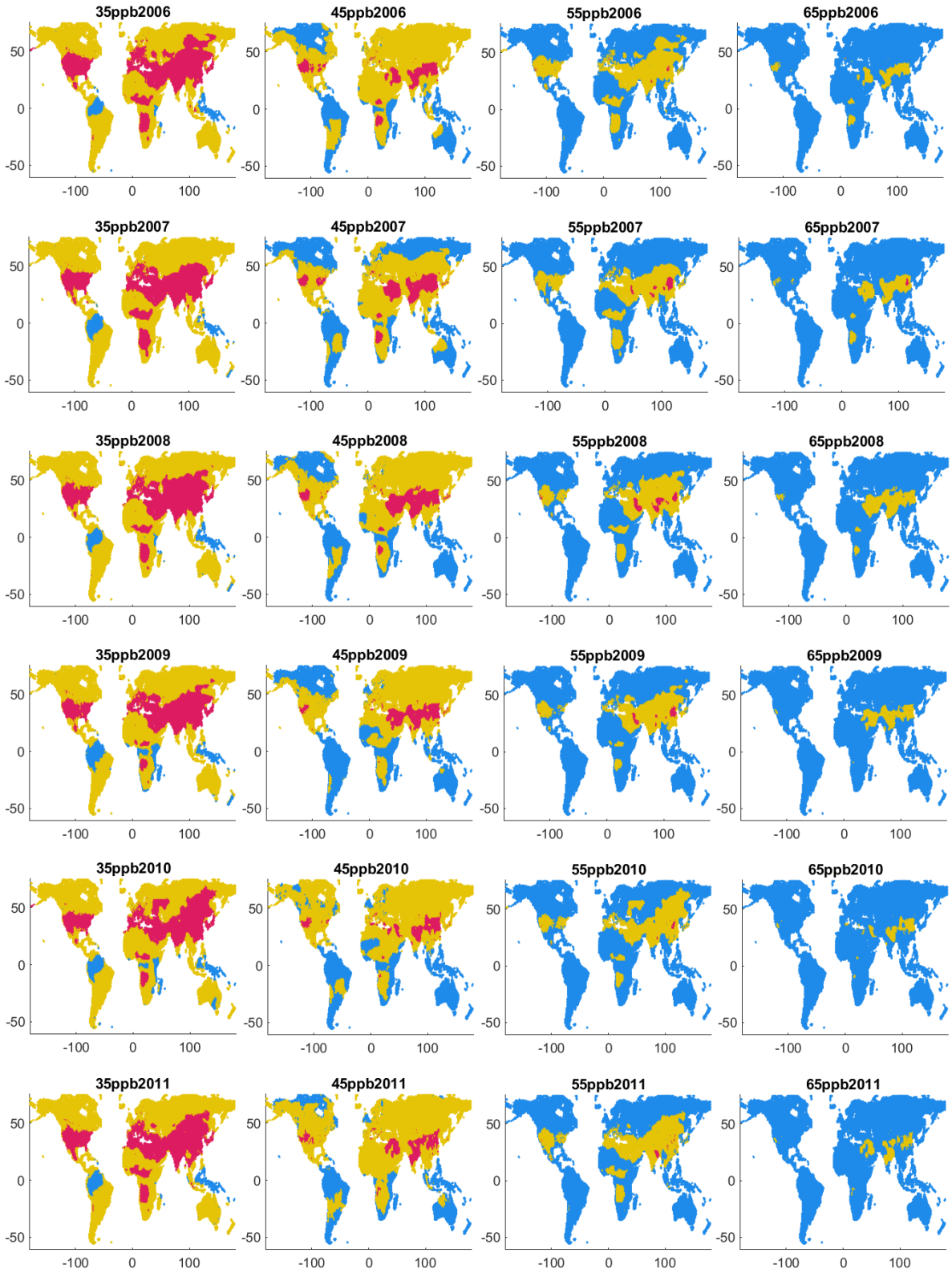
35ppb2006
45ppb2006
55ppb2006
65ppb2006
35ppb2007
45ppb2007
55ppb2007
65ppb2007
35ppb2008
45ppb2008
55ppb2008
65ppb2008
35ppb2009
45ppb2009
55ppb2009
65ppb2009
35ppb2010
45ppb2010
55ppb2010
65ppb2010
35ppb2011
45ppb2011
55ppb2011
65ppb2011
50
0
-50
-100
0
100

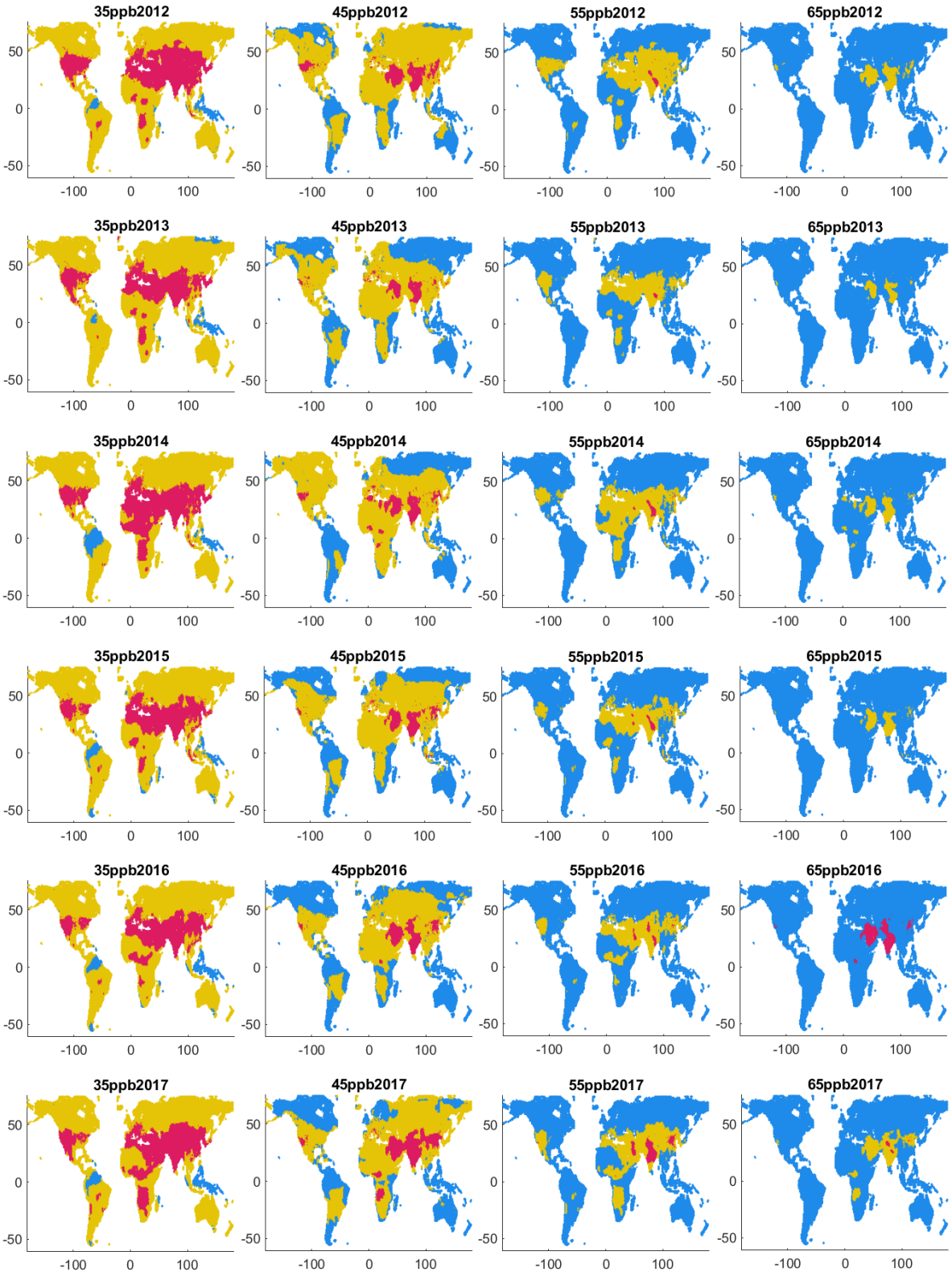
35ppb2012
45ppb2012
55ppb2012
65ppb2012
35ppb2013
45ppb2013
55ppb2013
65ppb2013
35ppb2014
45ppb2014
55ppb2014
65ppb2014
35ppb2015
45ppb2015
55ppb2015
65ppb2015
35ppb2016
45ppb2016
55ppb2016
65ppb2016
35ppb2017
45ppb2017
55ppb2017
65ppb2017
50
0
-50
-100
0
100

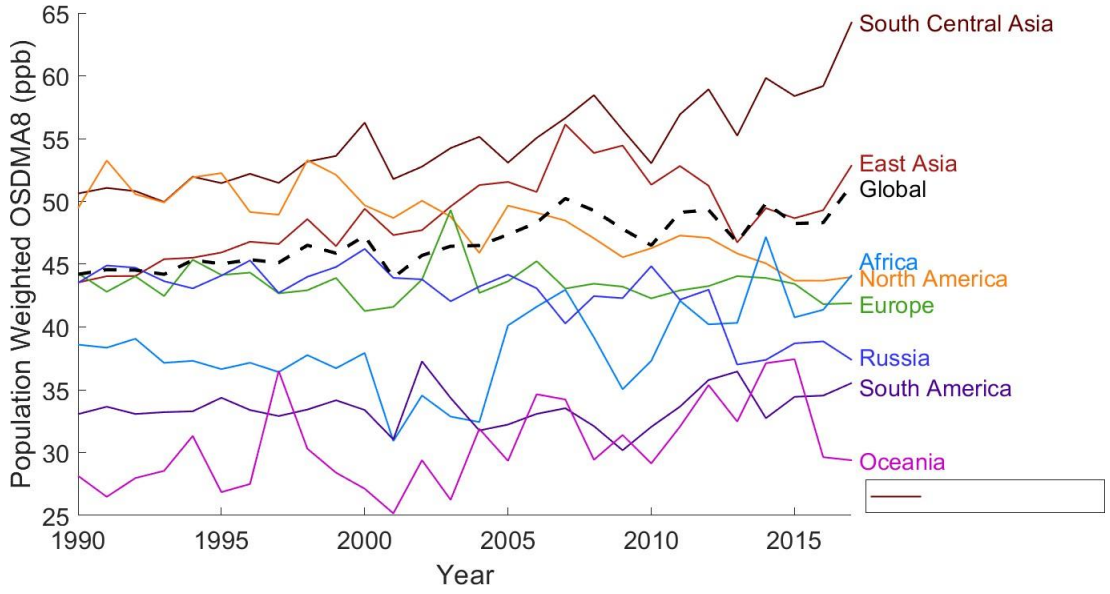

Figure S6. Ozone trends by region. Population weighted ozone rose from 1990 in Asia, which drove an overall global rise. North America had a clear downward trend while other regions slightly fluctuated but overall have no clear trend.

Table S1. Differences in ozone estimates caused by including RAMP. Differences between ozone estimates are shown in the final case where weighted RAMP is used before BME data fusion, minus results without using RAMP, in ppb (the results of DeLang et al., 2021). Results are shown for 2000 and 2017, for average difference and the absolute value of differences, for area-weighted and population-weighted results, and for the mean, median, and 5^{th} / 95^{th} percentiles. A positive value indicates that results using weighted RAMP are higher.

Year 2000

Region	Difference				Absolute Difference		
	5%ile	Mean	Median	95%ile	Mean	Median	95%ile
Africa	-0.018	0.004	0.001	0.048	0.012	0.002	0.061
East Asia	-0.029	0.199	0.036	0.869	0.233	0.051	0.908
Europe	-2.425	-0.273	-0.105	1.114	0.613	0.190	2.704
North America	-0.118	0.032	0.015	0.363	0.192	0.030	1.066
Oceania	-0.008	-0.000	-0.001	0.020	0.005	0.003	0.020
Russia	-0.042	0.012	0.000	0.131	0.026	0.003	0.141
South Central Asia	-0.018	0.006	0.007	0.026	0.012	0.008	0.035
South America	-0.007	0.012	0.006	0.057	0.014	0.007	0.057

Region	Population Weighted Difference				Population Weighted Absolute Difference		
	5%ile	Mean	Median	95%ile	Mean	Median	95%ile
Africa	-0.009	-0.000	0.000	0.009	0.010	0.001	0.050
East Asia	-0.163	0.294	0.078	0.913	0.337	0.166	0.934
Europe	-2.630	-0.205	-0.102	2.148	0.863	0.304	3.038
North America	-0.410	0.258	0.018	2.151	0.446	0.058	2.320
Oceania	-0.003	0.001	-0.000	0.017	0.002	0.001	0.017
Russia	-0.148	-0.033	-0.019	0.029	0.050	0.032	0.157

South Central Asia	-0.005	0.008	0.008	0.021	0.012	0.009	0.036
South America	-0.014	0.022	0.010	0.120	0.025	0.013	0.120

Year 2017

Region	Difference				Absolute Difference		
	5%ile	Mean	Median	95%ile	Mean	Median	95%ile
Africa	-0.642	-0.102	-0.000	0.018	0.114	0.013	0.652
East Asia	-1.868	0.140	0.043	2.776	0.855	0.420	3.057
Europe	-1.350	0.002	-0.005	1.469	0.488	0.192	2.024
North America	-0.088	0.013	0.007	0.118	0.042	0.014	0.176
Oceania	-0.002	0.011	0.001	0.063	0.012	0.001	0.062
Russia	-0.310	-0.044	-0.008	0.071	0.066	0.017	0.319
South Central Asia	-0.084	0.027	0.015	0.177	0.052	0.025	0.215
South America	-0.019	-0.001	0.002	0.011	0.008	0.003	0.020

Region	Population Weighted Difference				Population Weighted Absolute Difference		
	5%ile	Mean	Median	95%ile	Mean	Median	95%ile
Africa	-0.854	-0.101	0.001	0.017	0.111	0.007	0.854
East Asia	-1.916	0.217	0.148	2.560	0.897	0.563	2.736
Europe	-1.189	0.120	0.006	1.967	0.589	0.344	2.197
North America	-0.286	0.074	0.017	0.574	0.163	0.069	0.653
Oceania	0.000	0.033	0.024	0.091	0.033	0.024	0.091
Russia	-0.091	0.058	0.048	0.288	0.112	0.073	0.386
South Central Asia	-0.064	0.032	0.031	0.128	0.061	0.040	0.161
South America	-0.003	0.011	0.003	0.106	0.015	0.004	0.126

Table S2. Leave one out cross validation results. Results show that using RAMP decreases the mean square error (MSE) and increases R^2 over the M^3Fusion multi-model composite. When BME is used, the MSE and R^2 do not differ when using M^3Fusion as the global offset, or M^3Fusion bias-corrected using CAMP and weighted RAMP (wRAMP), which is expected because BME matches observations exactly at measurement stations, and many stations are clustered near one another.

Scenario	MSE (ppb^2)	R^2
Simple multi-model mean	189.23	0.28
M^3Fusion	61.14	0.30
CAMP	53.54	0.35
wRAMP	46.79	0.43
BME using M^3Fusion as offset (DeLang et al., 2021)	14.5	0.83
BME using CAMP as offset	14.5	0.83
BME using wRAMP as offset	14.5	0.83